

A Di-acidic (DXE) Code Directs Concentration of Cargo during Export from the Endoplasmic Reticulum*

(Received for publication, February 2, 1999, and in revised form, March 24, 1999)

Noriyuki Nishimura^{‡§¶}, Sergei Bannykh^{‡§}, Sarah Slabough[‡], Jeanne Matteson[‡],
Yoram Altschuler[¶], Klaus Hahn[‡], and William E. Balch^{‡§**}

From the Departments of [‡]Cell and [§]Molecular Biology, The Scripps Research Institute, La Jolla, California 92037 and the [¶]Department of Anatomy, University of California, San Francisco, California 941143

Efficient export of vesicular stomatitis virus glycoprotein (VSV-G), a type I transmembrane protein, from the endoplasmic reticulum requires a di-acidic code (DXE) located in the cytosolic carboxyl-terminal tail (Nishimura, N., and Balch, W. E. (1997) *Science* 277, 556–558). Mutation of the DXE code by mutation to AXA did not prevent VSV-G recruitment to pre-budding complexes formed in the presence of the activated form of the Sar1 and the Sec23/24 complex, components of the COPII budding machinery. However, the signal was required at a subsequent concentration step preceding vesicle fission. By using green fluorescence protein-tagged VSV-G to image movement in a single cell, we found that VSV-G lacking the DXE code fails to be concentrated into COPII vesicles. As a result, the normal 5–10-fold increase in the steady-state concentration of VSV-G in downstream pre-Golgi intermediates and Golgi compartments was lost. These results demonstrate for the first time that inactivation of the DXE signal uncouples early cargo selection steps from concentration into COPII vesicles. We propose that two sequential steps are required for efficient export from the endoplasmic reticulum.

selected for export by interacting with COPII coat components (3, 4). Selective recruitment of cargo to pre-budding protein complexes occurs in response to activation of the Sar1 GTPase to the GTP-bound form. This step is coordinated with the recruitment of the cytosolic Sec23/24 protein complex. These proteins, in combination with additional membrane proteins and the cytosolic Sec13/31 complex, promote membrane invagination and vesicle fission. Although some of the basic coat components involved in COPII coat assembly have been identified, the mechanism by which biosynthetic cargo is selected for and concentrated into COPII vesicles is unknown.

A role for sorting signals was first demonstrated for clathrin-mediated vesicle formation at the plasma membrane (reviewed in Ref. 5). Here, tyrosine-based motifs direct both the selection and concentration of cargo molecules into clathrin-coated vesicles through the interaction with the μ_2 chain of AP2 complexes (reviewed in Ref. 6). Similarly, the selection and concentration of recycling cargo into COPI-coated vesicles that mediate retrograde transport between Golgi compartments and from pre-Golgi compartments to the ER involve the KKXX motif (7) (reviewed in Ref. 8). Current evidence suggests that recycling cargo is concentrated by binding to the γ subunit of the COPI coat complex (9).

Signals involved in the selection of cargo for export from the ER are only beginning to emerge. Peptides containing a double Phe (FF) motif found in the cytoplasmic domain of the mammalian p24 family and p53/58 proteins that recycle between the ER and the Golgi have been shown to bind the Sec23 COPII component *in vitro* (10, 11). Mutation of these residues effects trafficking of these proteins *in vivo* (10, 12). Curiously, the FF motif in the yeast p24 family member Emp24p has been reported to attenuate the effect of a separate export signal composed of adjacent Leu-Val (LV) residues present at the extreme carboxyl terminus (13). We have recently found that a number of newly synthesized type 1 transmembrane proteins destined for the cell surface, including vesicular stomatitis glycoprotein (VSV-G), require a di-acidic motif (DXE) in their cytoplasmic domains for efficient export (14, 15). When the DXE code is mutated to AXA, VSV-G exits the ER at ~10-fold slower rates. Unlike the FF motif, the di-acidic code is sufficient to direct export from the ER. Addition of the code to the α subunit of the T-cell receptor- α , a resident ER protein, leads to recruitment into COPII vesicles (14). Although the code is necessary for efficient export, VSV-G transport is not completely blocked as the AXA mutant exits the ER with ~10-fold reduced efficiency (14). This raises the possibility that the DXE signal participates in only a subset of interactions required for the efficient coupling of biosynthetic cargo to the ER export machinery.

Whereas clathrin recognizes fully folded cargo for selective delivery to distinct destinations, export of newly synthesized cargo from the ER is faced with competing pathways including

Multiple pathways in the endoplasmic reticulum (ER),¹ including folding and degradation, compete for transport of newly synthesized cargo to the Golgi. What are the molecular mechanisms directing efficient export? Movement of cargo between compartments of the secretory pathway involves selective sorting and concentration into vesicle carriers (1). Newly synthesized cargo that is translocated into the ER is incorporated into COPII-coated vesicles (2). Cargo exiting the ER includes both endogenous transport components that must be recycled from post-ER compartments for reuse and biosynthetic proteins that are delivered to downstream subcellular destinations and the cell surface. Cargo is sorted from resident ER proteins and

* This work was supported by National Institutes of Health Grant GM 42336 (to W. E. B.) and by Core C of the National Cancer Institute Grant CA 58689. The costs of publication of this article were defrayed in part by the payment of page charges. This article must therefore be hereby marked "advertisement" in accordance with 18 U.S.C. Section 1734 solely to indicate this fact.

[¶] Senior Postdoctoral Fellow of the American Cancer Society.

** To whom correspondence should be addressed: Depts. of Cell and Molecular Biology, The Scripps Research Institute, 10550 N. Torrey Pines Rd., La Jolla, CA 92037. Tel: 619-784-2310; Fax: 619-784-9126; E-mail: webalch@scripps.edu.

¹ The abbreviations used are: ER, endoplasmic reticulum; VSV-G, vesicular stomatitis virus glycoprotein; endo H, endoglycosidase H; BHK, baby hamster kidney; NRK, normal rat kidney; GFP, green fluorescent protein; GST, glutathione S-transferase; HRP, horseradish peroxidase; HA, hemagglutinin; PBS, phosphate-buffered saline; GS beads, glutathione-Sepharose beads; BSA, bovine serum albumin; Syn5, syntaxin 5; SFV, Semliki forest virus; TGN, trans Golgi network.

those directing completion of folding ("quality control" (16)) and those that target proteins for degradation (17). Moreover, unlike clathrin-mediated carriers, ER-derived vesicles are delivered to a common destination, the Golgi stack. Thus, cargo sorting from the ER is a problem unique to the COPII machinery. The functional relationships between signals that target biosynthetic cargo to each of the ER-specific pathways are unknown. Signal strength for each route will be expected to affect the kinetics of export from the ER. Moreover, it is now evident that a number of endogenous factors, some of which recycle between the ER and the Golgi, temporally associate with biosynthetic cargo and are essential for export (18–22). Thus, multiple signals on cargo may be required to direct interaction with specialized accessory factors as well as the general COPII machinery to solicit efficient export.

We have recently shown that VSV-G interacts with a subset of COPII components, the Sar1 GTPase and the Sec23/24 complex, to form pre-budding complexes that are subsequently assembled in mature COPII vesicles budding from the ER (3). From these and related studies in yeast (4), it is clear that components of the COPII machinery participate in cargo selection and concentration. Whether the DXE signal directs the initial selection event, concentration, or both remains a fundamental question that needs to be addressed.

To analyze the mechanism of the DXE signal in cargo selection and concentration during ER export, we have taken advantage of cells expressing VSV-G. The transport of VSV-G has been extensively utilized to define the basic biochemical components and principles of operation of the secretory pathway (reviewed in Refs. 1 and 15). In particular, the tsO45 strain of VSV-G (VSV-G^{ts}) can be accumulated in the ER due to a temperature-sensitive folding defect when cells are incubated at the restrictive temperature of 39.5 °C. Upon shift to the permissive temperature of 32 °C its folding resumes, allowing VSV-G^{ts} to exit the ER. The ability to synchronize movement of VSV-G^{ts} allows us to follow a single well defined biosynthetic cargo molecule through the secretory pathway (3, 23–26).

In order to visualize export directly from the ER, we have tagged both the tsO45-VSV-G wild-type (G^{ts}-DXE) and the AXA mutant (G^{ts}-AXA) with green fluorescence protein (GFP). By monitoring the real time movement of GFP-VSV-G^{ts} within the same cell *in vivo* and *in vitro* using video microscopy, we find that the DXE motif plays a key role in the concentration of VSV-G into COPII-coated vesicles at ER export sites. Loss of concentration of the AXA mutant is not a consequence of inability of the mutant to be recruited to pre-budding complexes formed in the presence of activated Sar1 and Sec23/24. Our ability to uncouple cargo selection by the COPII machinery from a downstream concentration event(s) preceding vesicle fission leads us to propose a minimal two-step model for ER export of cargo.

EXPERIMENTAL PROCEDURES

Reagents—Texas Red goat anti-mouse and anti-rabbit IgG conjugates were obtained from Molecular Probes (Eugene, OR). Horseradish peroxidase (HRP)-conjugated Fab fragments of goat anti-rabbit antibodies were purchased from BioSys (Compiègne, France). Anti-HA antibody (12CA5) was obtained from Roche Molecular Biochemicals. Polyclonal antibodies recognizing α -1,2-mannosidase II, green fluorescence protein (GFP), and a luminal domain of VSV-G were generous gifts from M. Farquhar (University of California, San Diego, CA), C. Zukar (University of California, San Diego, CA), and K. Simons (EMBL, Heidelberg, Germany), respectively. A monoclonal antibody recognizing a luminal domain of VSV-G (8G5) was kindly provided by B. Wattenberg (Upjohn, Kalamazoo, MI). Polyclonal antibodies against a cytoplasmic tail of VSV-G (T251) and syntaxin 5 (Syn5) was described previously (27, 28). Purified proteins of GST-Sar1 H79G and Sec23/24 complex were prepared as described (3). Recombinant adenovirus and Semliki forest virus (SFV) were generated using the method described in Ref. 29

and SFV gene expression system kit (Life Technologies, Inc.), respectively. All other reagents were purchased from Sigma.

DNA Constructs—The carboxyl terminus of tsO45-VSV-G wild-type (G^{ts}-DXE) and AXA mutant (G^{ts}-AXA) (14) were tagged with Myc and HA epitope by polymerase chain reaction. The resulting clones (Myc-G^{ts}-DXE and HA-G^{ts}-AXA) were subcloned into pAdtet7 vector for recombinant adenovirus production. The S65T variant of GFP (30) was fused to the carboxyl terminus of G^{ts}-DXE or G^{ts}-AXA with an amino acid spacer (Ala) by standard two-step polymerase chain reaction (31). The resulting clones (GFP-G^{ts}-DXE and GFP-G^{ts}-AXA) were subcloned into pSFV3 vector for recombinant SFV production. All constructs used in this study were verified by DNA sequencing.

Pre-budding Complex Isolation—Microsomes were prepared from recombinant adenovirus (Myc-G^{ts}-DXE or HA-G^{ts}-HA)-infected tTA-HeLa cells as described (27, 29). Pre-budding complex isolation was performed as described (3). Briefly, microsomes (180–200 μ g) were salt-washed and incubated in a transport buffer containing GST-Sar1 H79G (7 μ g), Sec23/24 (5 μ g), and 1 mM GTP for 30 min at the indicated temperature. The microsomes were collected by centrifugation and solubilized by 1% digitonin. Subsequently pre-budding complex containing GST-Sar1 H79G was isolated on GS beads. Myc-G^{ts}-DXE and HA-G^{ts}-AXA recovered in pre-budding complex were determined by Western blotting as described below.

Western Blotting—For pre-budding complex isolation, eluates from GS beads and 1/4 of the total lysate were separated by 7.5% SDS-polyacrylamide gel electrophoresis, transferred to nitrocellulose membranes, and immunoblotted using T251 (for Myc-G^{ts}-DXE) or 12CA5 (for HA-G^{ts}-AXA) antibody. For GFP-G^{ts}-DXE and GFP-G^{ts}-AXA expression, BHK cell lysates were immunoblotted using anti-GFP antibody. Blots were developed using an ECL kit (Amersham Pharmacia Biotech) and quantitated using a Densitometer SI (Molecular Dynamics, Sunnyvale, CA).

Indirect Immunofluorescence—Indirect immunofluorescence was performed as described (26). Cells were fixed in 2% formaldehyde in PBS and blocked with 5% goat serum in PBS (PBS/goat serum). To detect VSV-G reached to the cell surface, cells were incubated with a monoclonal antibody against VSV-G (8G5) in the absence of saponin and visualized with Texas Red goat anti-mouse IgG conjugate. To detect α -1,2-mannosidase II and Syn5, cells were permeabilized with 0.1% saponin in goat serum/PBS, incubated with an appropriate antibody in the presence of 0.1% saponin, and visualized with Texas Red goat anti-rabbit IgG conjugate. Images were recorded digitally and quantified as described below.

Immunoelectron Microscopy—For immunoperoxidase cytochemistry, cells were fixed in 3% formaldehyde, 0.025% glutaraldehyde in PBS for 60 min, washed with PBS containing 0.05 M glycine, and permeabilized with 0.05% saponin in PBS containing 0.2% BSA (PBS/BSA). Then cells were incubated with a polyclonal antibody against VSV-G overnight at 4 °C and with HRP-conjugated secondary antibodies for 2 h. After several washes with PBS/BSA, cells were fixed with 2.5% glutaraldehyde in 0.1 M sodium cacodylate (pH 7.4) for 30 min, washed with 0.1 M Tris/HCl (pH 7.2), and incubated with 1 mg/ml diaminobenzidine in 0.1 M Tris/HCl (pH 7.2) containing 0.01% H₂O₂ for 10 min. After washing out diaminobenzidine to terminate HRP reaction, cells were postfixed in 0.1 M sodium cacodylate (pH 7.4), cacodylate containing 1% reduced OsO₄, and 1% KFeCN. Finally cells were treated with 1% tannic acid for 1 h, dehydrated, and embedded in Epon 812 as described (38). Thin sections were cut as described (38), stained with lead citrate, and viewed on JEOL 1200EX-II electron microscope (JEOL, Peabody, MA) at 80 kV. In order to quantitate the effects of DXE mutation, 25 cells expressing VSV-G in the ER were chosen, and all of the Golgi stacks within these cells were examined for the presence of HRP reaction products. Immunogold (6 nm) electron microscopy and quantification were performed as described (32).

Imaging of Fluorescence—Indirect immunofluorescence and time lapse imaging of GFP was performed using an inverted microscope (Carl Zeiss Axiovert 100TV, Thornwood, NY) equipped with a CCD camera (Photometrics PXL, Tucson, AZ), a motorized objective lens (Carl Zeiss, Thornwood, NY), a temperature controller (20/20 Technology Inc., Wilmington, NC), and an automated stage (Ludl Electronic Products Ltd., Hawthorne, NY). Isee (Inovision, Raleigh, NC) was used to control both image acquisition and an automated stage on a UNIX computer (Silicon Graphics O2; Mountain View, CA). Pixel intensities of ER, pre-Golgi intermediates, and Golgi were determined from raw data using NIH Image 1.62 program.

Morphological Analysis of Transport *in Vivo*—Morphological analysis of VSV-G transport *in vivo* was performed as described (33). Briefly, BHK cells on coverslips in 35-mm dish were infected with recombinant

vaccinia virus encoding T7 RNA polymerase (ν TF7-3) and transfected with pAR plasmid encoding either GFP-tagged G^{ts} -DXE (GFP- G^{ts} -DXE) or G^{ts} -AXA (GFP- G^{ts} -AXA) at 39.5 °C. After 6 h transfection, cells were subjected to either indirect immunofluorescence, immunoelectron microscopy, or time-lapse imaging. For indirect immunofluorescence and immunoelectron microscopy, transport was initiated by transferring cells to 15, 20, or 32 °C and terminated by transferring to ice. For time-lapse imaging, cells were put on an automated stage pre-equilibrated at 4 °C and overlaid with an ice-cold medium without phenol red. Transport was initiated by raising its temperature to 32 °C, and time-lapse images of one cell were acquired every 1 min up to 120 min.

Morphological Analysis of Transport *in Vitro*—Morphological analysis of VSV-G transport *in vitro* was performed as described (26). Briefly, NRK cells on coverslips in 35-mm dish were infected with recombinant SFV encoding either GFP- G^{ts} -DXE or GFP- G^{ts} -AXA at 39.5 °C. After 24 h infection, cells were permeabilized with digitonin, transferred to an automated stage pre-equilibrated at 4 °C, and overlaid with a transport mixture (25 mM Hepes/KOH (pH 7.2), 75 mM KOAc, 2.5 mM Mg(OAc)₂, 5 mM EGTA, 1.8 mM CaCl₂, 1 mM ATP, 5 mM creatine phosphate, 0.2 IU rabbit muscle creatine phosphokinase, 2.5 mg/ml rat liver cytosol (34)). Before initiating transport by raising the temperature to 32 °C, 10 cells were identified, and their positions were recorded by an Isee (Inovision, Raleigh, NC) automated stage controller. Subsequently transport was initiated, and time-lapse images of each cell were acquired every 10 min up to 60 min.

RESULTS

The Role of the Di-acidic Exit Code in Recruitment of VSV-G into Pre-budding Complexes—VSV-G is a type I transmembrane glycoprotein containing two N-linked oligosaccharides in the luminal domain and a 29-amino acid cytoplasmic tail. We have recently shown that the cytoplasmic tail of VSV-G contains a di-acidic export signal (DXE) that is sufficient to direct the export of cargo from the ER (14). Substitution of this DXE code with Ala (AXA) results in an ~5–10-fold reduction in the rate of ER export based on the kinetics of processing of its N-linked oligosaccharides from endoglycosidase H (endo H)-sensitive species found in the ER to endo H-resistant forms found in the cis/medial Golgi compartments. Consistent with the reduced rate of processing in Golgi, we have shown that at an early time point (10 min) following temperature shift, only trace levels of the AXA mutant can be detected in the Golgi stack using indirect immunofluorescence (14). However, this mutation does not affect the total extent of the transport. Pulse-labeled AXA mutant present in the ER can be recovered in fully processed Golgi forms at longer incubation times (60–90 min) (14).

To begin to explore the mechanism by which the DXE signal directs efficient ER export, we first examined whether the DXE code was necessary for the recovery of VSV-G in detergent-soluble pre-budding complexes. These are intermediates in the pathway required for the selection and concentration of VSV-G in COPII vesicles (3). Recovery in pre-budding complexes is specific as ER resident proteins are efficiently excluded from these intermediates (3). They can be readily detected when ER membranes are incubated in the presence of a subset of COPII components, the Sec23/24 complex and a glutathione S-transferase (GST)-tagged Sar1[H79G], a mutant that has a markedly reduced rate of GTP hydrolysis (Sar1-GTP) (27). Sar1-GTP stabilizes the assembled pre-budding complex for isolation on glutathione-Sepharose (GS) beads in the presence of detergent (3). We have recently demonstrated that interaction of cargo with these COPII components precedes completion of folding and oligomerization, suggesting that recruitment to pre-budding complexes represents an early step in the export pathway (32).

To generate ER microsomes containing wild-type or AXA mutant VSV-G, tTA-HeLa cells were infected with recombinant adenovirus expressing either Myc-tagged VSV- G^{ts} -DXE (Myc- G^{ts} -DXE) or HA-tagged VSV- G^{ts} -AXA (HA- G^{ts} -AXA). VSV- G^{ts}

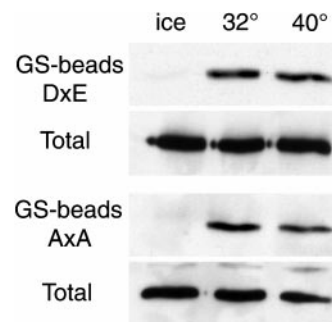


FIG. 1. The AXA mutant can be recovered in pre-budding complexes. Microsomes prepared from tTA-HeLa cells infected with recombinant adenovirus expressing either Myc- G^{ts} -DXE or HA- G^{ts} -AXA were incubated in the presence GST-Sar1-GTP and purified Sec23/24 complex on ice at 32 or 40 °C. Subsequently, detergent-soluble pre-budding complexes were recovered on GS beads. VSV-G in the pre-budding complex was detected by immunoblotting as described under “Experimental Procedures.” Total VSV-G represents 1/4 of the total lysate used for isolation of pre-budding complexes. Quantitation reported in the text was determined by densitometry.

(G^{ts}) is a temperature-sensitive variant of wild-type G protein produced by tsO45 virus. VSV- G^{ts} fails to exit the ER when cells expressing the protein are incubated at the restrictive temperature (39.5 °C). Transfer of cells to the permissive temperature (32°) leads to synchronous export (24, 26, 33). The ability to synchronize export allows us to control the movement of VSV-G from the ER into early compartments of the secretory pathway including pre-Golgi intermediates and Golgi cisternae (23, 24, 26, 34). We have used VSV-infected cells expressing G^{ts} extensively to demonstrate the central role of the Sar1 GTPase and other COPII components in the formation of VSV-G containing COPII-coated vesicles (3, 14, 27). Neither the Myc nor the HA tags were found to have any effect on the kinetics of transport of the untagged G^{ts} -DXE or G^{ts} -AXA mutant to the Golgi based on processing to endo H-resistant forms (data not shown).

Following infection at the restrictive temperature to restrict either the Myc- G^{ts} DXE or HA- G^{ts} AXA to the ER, microsomes were prepared and incubated *in vitro* 30 min in the presence of GST-Sar1-GTP and Sec23/24 as described (3) to generate pre-budding complexes. As expected, Myc- G^{ts} DXE was not recovered in pre-budding complexes when microsomes were incubated on ice, a condition that also does not support COPII recruitment or vesicle budding from the ER (27) (Fig. 1). In contrast, Myc- G^{ts} -DXE was recovered at both the permissive and restrictive temperatures (~18% of total based on quantitative immunoblotting) (Fig. 1). This result is consistent with our recent observations that untagged VSV- G^{ts} can be efficiently captured in pre-budding complexes in both the folded and unfolded states (32).

Interestingly, the HA- G^{ts} -AXA was also efficiently recovered in the pre-budding complexes formed in the presence of Sar1-GTP at both the permissive and restrictive temperatures (~20% of total) (Fig. 1). Under these conditions less than 10% of the HA- G^{ts} -AXA has exited the ER at the permissive temperature compared with >90% for Myc- G^{ts} -DXE (14). Although we were surprised at our ability to recover VSV-G in pre-budding complexes given the possibility that it was a COPII recognition motif (14), this suggests that the DXE code is also required for a new, previously undetected, step after formation of pre-budding complexes to promote efficient ER export.

Inactivation of the Di-acidic Exit Code Markedly Reduces the Steady-state Concentration of VSV-G in Golgi Compartments—To identify novel step(s) requiring DXE function for accelerated ER export, we tagged the tsO45 variant of VSV-G with green fluorescent protein (GFP) (GFP- G^{ts}) in order to

follow transport in real time in single cells using fluorescence microscopy (35). Baby hamster kidney (BHK) cells were transiently transfected with GFP-G^{ts} containing either the wild-type DXE exit code (GFP-G^{ts}-DXE) or the mutant (GFP-G^{ts}-AXA). Both the GFP-G^{ts}-DXE and GFP-G^{ts}-AXA were restricted to the ER when cells were incubated at 39.5 °C based on sensitivity to endo H and ER localization using indirect immunofluorescence (data not shown; see below). Transfer to the permissive temperature resulted in the processing of GFP-G^{ts}-DXE and GFP-G^{ts}-AXA to endo H-resistant forms. The kinetics of processing of GFP-tagged G^{ts} paralleled that of their respective untagged wild-type and mutant forms (14) (data not shown). These results demonstrate that the tag has no effect on the overall properties or kinetics of transport of tsO45 VSV-G as observed previously (35). When transiently transfected cells were analyzed using immunoblotting, we found that the GFP-G^{ts}-AXA construct was expressed on average at an ~2-fold greater efficiency than that of the GFP-G^{ts}-DXE (Fig. 2A, inset in panel a).

To determine the steady-state distribution of wild-type and mutant VSV-G, following transfection at 39.5 °C to accumulate protein in the ER, cells were incubated at the permissive temperature of 32 °C for 120 min. This time frame is sufficient to mobilize both mutant and wild-type forms of VSV-G to the cell surface (14). Under these conditions we found that GFP-G^{ts}-DXE showed the typical increased fluorescence in Golgi compartments over that observed in the ER (Fig. 2A, panel a). Golgi localization of concentrated GFP-G^{ts}-DXE was confirmed by co-localization with the cis/medial Golgi marker protein α -1,2-mannosidase II (36, 37) (Fig. 2A, panel b). Thus, the addition of the GFP tag to the cytoplasmic tail does not interfere with efficient delivery of GFP-G^{ts}-DXE into COPII vesicles during export from the ER.

In contrast to GFP-G^{ts}-DXE, delivery of GFP-G^{ts}-AXA to the Golgi was difficult to detect using indirect immunofluorescence despite its ~2-fold expression relative to GFP-G^{ts}-DXE (Fig. 2A, panel c). The normal distribution observed for α -1,2-mannosidase II in GFP-G^{ts}-AXA transfected cells (Fig. 2A, panel d) excludes the possibility that expression of GFP-G^{ts}-AXA *per se* disturbs the organization of Golgi compartments.

These results are quantitated in Fig. 2B where GFP-G^{ts}-DXE was found to be concentrated 7.2-fold relative to the ER (Fig. 2B, lane a), whereas the GFP-G^{ts}-AXA mutant was detected at levels 1.2-fold that found in the ER (Fig. 2B, lane b). No difference in the relative concentration of the α -1,2-mannosidase II marker compared with background was detected in GFP-G^{ts}-DXE- or GFP-G^{ts}-AXA-expressing cells (Fig. 2B, lanes c and d). Importantly, the lack of concentration of GFP-G^{ts}-AXA in Golgi compartments did not reflect a defect in the ability of the mutant to be transported to and through the Golgi stack. GFP-G^{ts}-AXA could readily be detected on the cell surface at levels comparable to that of wild type (Fig. 2C). Because concentration of cargo does not occur during transit of cargo between compartments of the Golgi stack (24, 38), these results raise the possibility that the DXE motif may be required for concentration during ER export.

GFP-G^{ts}-AXA Is Not Concentrated in the TGN at 20 °C—GFP-G^{ts}-AXA failed to be concentrated in Golgi compartments in cells incubated at 32 °C relative to levels observed in the ER. It remained possible that we could not detect this event morphologically due to a more rapid transport of GFP-G^{ts}-AXA from the Golgi to the cell surface compared with its rate of export from the ER. To address this concern, we took advantage of the well established effects of incubation at 20 °C on exit from the Golgi stack. At 20 °C, the transport of VSV-G and other cargo are kinetically inhibited in the trans Golgi network

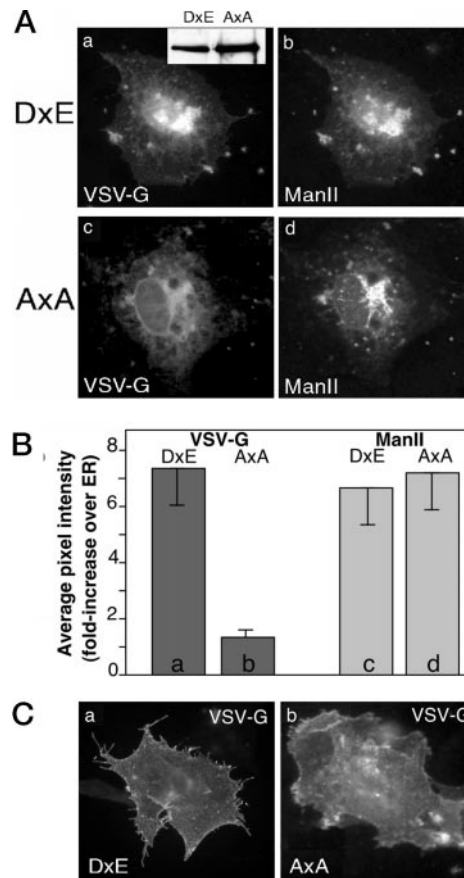


FIG. 2. The AXA mutant is not concentrated in the Golgi at steady state. A, BHK cells were transfected with either GFP-G^{ts}-DXE or GFP-G^{ts}-AXA at 39.5 °C. Following transfection, cells were shifted to 32 °C for 120 min to reach steady state where both mutant and wild-type protein are distributed throughout the entire exocytic pathways. The relative concentration of VSV-G in the exocytic compartments was determined by following the distribution of GFP as described under "Experimental Procedures." α -1,2-Mannosidase II (*ManII*) was visualized using specific antibody as described under "Experimental Procedures." Results are representative of over 100 cells examined. Inset, BHK cells were transfected with either GFP-G^{ts}-DXE or GFP-G^{ts}-AXA at 39.5 °C. Following transfection, the amount of VSV-G was determined using immunoblotting as described under "Experimental Procedures." B, quantitation of concentration in response to mutation of the DXE signal. Average pixel intensity of Golgi and ER was determined as described under "Experimental Procedures." The fold increase relative to ER is indicated. The error bars indicate the standard deviation of the mean for over 25 individual determinations. C, GFP-G^{ts}-AXA can be readily detected at the cell surface. BHK cells were transfected with either GFP-G^{ts}-DXE (panel a) or GFP-G^{ts}-AXA (panel b) at 39.5 °C. Following transfection, cells were shifted to 32 °C for 120 min to reach the cell surface. VSV-G at the cell surface was visualized by indirect immunofluorescence as described under "Experimental Procedures." Results are representative of over 100 cells examined.

(TGN) with little transport to the cell surface (39). This results in the accumulation of cargo in the TGN and elaboration of the trans-most tubular elements of the Golgi.

When cells transfected with GFP-G^{ts}-DXE were transferred from 39.5 to 20 °C for 120 min, GFP-G^{ts}-DXE accumulated in the TGN as expected (Fig. 3A, panel a). In contrast, GFP-G^{ts}-AXA showed only a slight increase in fluorescence over the background ER levels (Fig. 3A, panel b). The apparent slight increase is likely to be due to the overlapping elements of the Golgi stack that are frequently found in compacted forms in peri-nuclear loci. In this experiment, GFP-G^{ts}-DXE was concentrated 5.5-fold relative to the ER level (Fig. 3C, lane a), whereas the AXA was found at 1.4-fold that observed in the ER (Fig. 3C, lane b). Thus, incubation at 20 °C failed to show any

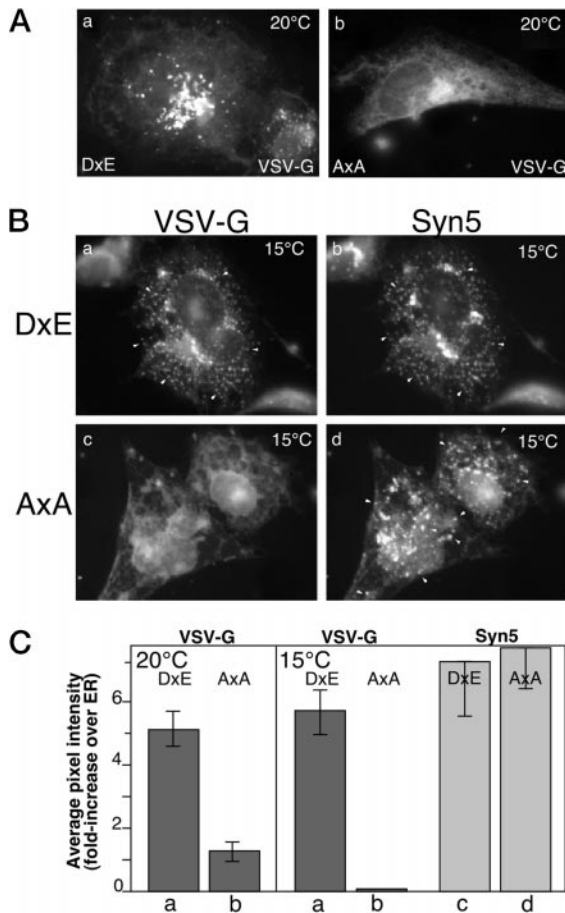


FIG. 3. GFP-G^{ts}-AXA is not concentrated in post-ER compartments at reduced temperature. A, GFP-G^{ts}-AXA is not concentrated in the TGN at 20 °C. BHK cells were transfected with either GFP-G^{ts}-DxE (panel a) or GFP-G^{ts}-AXA (panel b) at 39.5 °C. Following transfection, cells were shifted to 20 °C for 120 min to prevent the export of VSV-G from the TGN. The distribution of VSV-G was determined by detecting the fluorescence of GFP as described under “Experimental Procedures.” Results are representative of over 100 cells examined. B, GFP-G^{ts}-AXA is not concentrated in the pre-Golgi intermediates at 15 °C. BHK cells were transfected with either GFP-G^{ts}-DxE (panels a and b) or GFP-G^{ts}-AXA (panels c and d) at 39.5 °C. Following transfection, cells were shifted to 15 °C for 120 min to block the transport from the pre-Golgi intermediates to the cis Golgi compartment. The distribution of VSV-G (panels a and c) was determined by detecting the fluorescence of GFP. Syn5 was visualized using specific antibody as described under “Experimental Procedures” (panels b and d). The arrowheads indicate pre-Golgi intermediates. Results are representative of over 100 cells examined. C, quantitation of concentration in response to mutation of the DXE signal. Average pixel intensity of pre-Golgi intermediates and ER were determined as described under “Experimental Procedures.” The fold increase relative to ER is indicated. The error bars indicate the standard deviation of the mean for over 25 individual determinations.

significant concentration of GFP-G^{ts}-AXA in trans-most Golgi compartments.

GFP-G^{ts} AXA Is Not Concentrated in Pre-Golgi Intermediates at 15 °C—Although the inability to detect concentrated VSV-G in Golgi compartments is consistent with a role for the DXE code in directing concentration during ER export, it is necessary to directly assess its effect on the movement of VSV-G from the ER. For this purpose, we took advantage of previous studies where we and others (26, 38, 40, 41) have demonstrated that cargo exiting the ER in COPII vesicles accumulates in numerous punctate pre-Golgi intermediates. These consist of compact clusters of vesicular-tubular elements that form when cells are incubated at the reduced temperature of 15 °C. Current evidence suggests that the tubular elements

are likely to arise from the fusion of COPII vesicles (34) that can be readily visualized using indirect immunofluorescence (23, 26, 40, 42). Visualization of the dynamic movement of pre-Golgi intermediates containing GFP-VSV-G^{ts} on microtubules in living cells (35) has shown that peripheral vesicular-tubular clusters function to deliver cargo to the central Golgi region (reviewed in Ref. 15).

When BHK cells transfected with GFP-G^{ts}-DxE at 39.5 °C were incubated at 15 °C for 120 min, they showed the typical accumulation of VSV-G in numerous punctate structures throughout the cell (Fig. 3B, panel a). These co-localized with the pre-Golgi intermediate marker protein syntaxin 5 (Syn5) (Fig. 3B, panel b) (34). In contrast, in GFP-G^{ts}-AXA-transfected cells no structures containing GFP (Fig. 3B, panel c) could be observed, despite the abundance of Syn5-containing elements (Fig. 3B, panel d). On average, the number of Syn5-containing elements that accumulate at 15 °C in GFP-G^{ts}-AXA-transfected cells was the same as that observed in GFP-G^{ts}-DxE-transfected cells (~60–100 punctate elements per cell). This indicates that transfection with GFP-G^{ts}-AXA did not affect the ability of the cell to generate Syn5-containing pre-Golgi intermediates at 15 °C. When quantitated, GFP-G^{ts}-DxE was concentrated 5.8-fold over that observed in the ER (Fig. 3C, lane a), whereas an increase in GFP-G^{ts}-AXA concentration was not detectable (Fig. 3C, lane b). The concentration of Syn5 in pre-Golgi intermediates that accumulate at 15 °C were identical in GFP-G^{ts}-DxE- and GFP-G^{ts}-AXA-expressing cells (Fig. 3C, lanes c and d). The inability to detect concentrated GFP-G^{ts}-AXA in pre-Golgi intermediates under conditions where these structures form normally provides direct evidence that DXE participates in the efficient delivery to these structures.

Real Time Imaging Confirms the Requirement for the DXE Code in Concentration—The above results utilized fixed time points to visualize directly the distribution of VSV-G morphologically *in vivo*. It remained possible that the movement of GFP-G^{ts}-AXA through pre-Golgi intermediates to the Golgi was a transient event. Moreover, incubation at reduced temperature may have in some unexpected way exacerbated the reduced kinetics of transport of the AXA mutant. To circumvent these potential concerns, we examined the continuous real time movement of GFP-G^{ts}-DxE and GFP-G^{ts}-AXA in living cells over a complete time course of 120 min.

BHK cells were transfected with either GFP-G^{ts}-DxE or GFP-G^{ts}-AXA at 39.5 °C to restrict the protein to the ER. Subsequently, cells were shifted to the permissive temperature, and the movement of VSV-G was followed in real time using fluorescence video microscopy. Representative time frames are shown in Fig. 4. GFP-G^{ts}-DxE showed rapid concentration in pre-Golgi intermediates (Fig. 4, a–e) as reported previously (35). This was particularly evident by the 10-min (Fig. 4d, arrowheads) and 15-min (Fig. 4e, arrowheads) time points. In contrast, no detectable concentration of GFP-G^{ts}-AXA was observed in any structure during a 45-min incubation at 32 °C (Fig. 4, f–j) or up to 120 min of incubation (data not shown). This is a time period sufficient for complete processing of pulsed GFP-G^{ts}-AXA in the ER to Golgi-modified endo H-resistant forms (14) and for efficient delivery to the cell surface (Fig. 4j, arrow; Fig. 2C) (14). A real time visualization of export of GFP-G^{ts}-DxE and GFP-G^{ts}-AXA to pre-Golgi intermediates can be found on the Internet.²

The appearance of VSV-G in pre-Golgi intermediates was quantitated over a time course of 75 min (Fig. 5, closed circles). Following a brief lag period, the number of VSV-G containing

² The on-line address is as follows: www.scripps.edu/cb/balch/dxeparper. (User, balch) (password, ER).

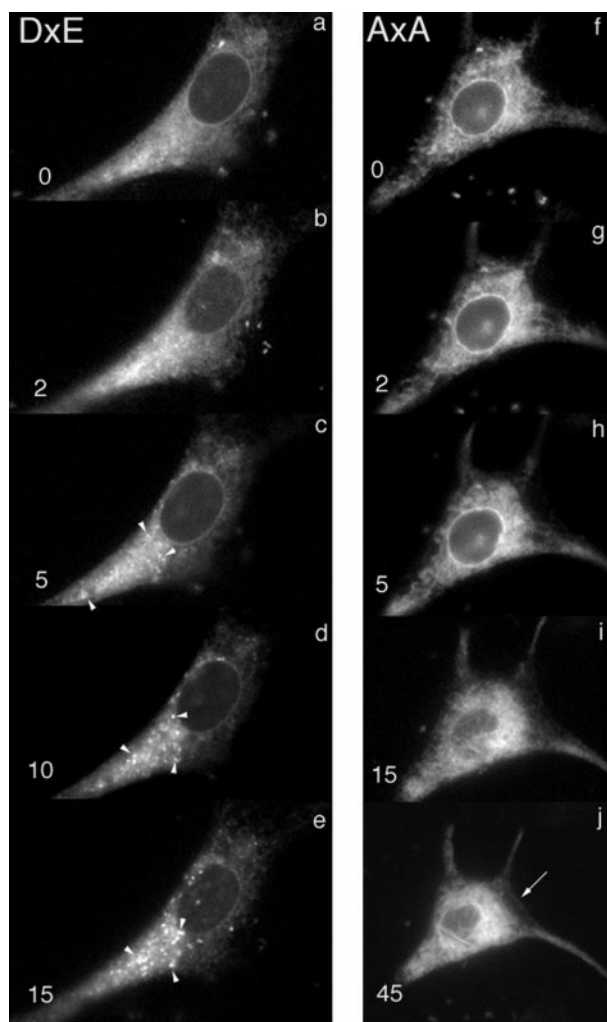


FIG. 4. GFP-G^{ts}-AXA is not concentrated during export from the ER at 32 °C. BHK cells transfected with either GFP-G^{ts}-DXE (a–e) or GFP-G^{ts}-AXA (f–j) at 39.5 °C were transferred directly to ice. Transport was initiated by shifting cells from ice to 32 °C. Time-lapse images of VSV-G within a living cell were acquired as described under “Experimental Procedures.” The arrow in *j* indicates the cell surface. The images can be visualized in real time.²

punctate structures increased with time to a peak level of ~50 elements at the 30-min time point which declined slightly to a steady-state level of ~45 in this typical series. This number is consistent with the average number of pre-Golgi intermediates detectable in living cells using quantitative stereology (38). The slight decline in intermediates may reflect consolidation of VSV-G in the more perinuclear Golgi regions following microtubule-mediated transit to this region of the cell (35). In contrast, no detectable intermediates containing concentrated VSV-G were discernible at any time point (Fig. 5, open circles). These *in vivo* data are consistent with an essential role for the DXE motif in concentration of VSV-G in COPII vesicles.

The Reduced Concentration of GFP-G^{ts}-AXA in the Golgi Can Be Detected by Electron Microscopy—To analyze the effects of the di-acidic code on the concentration of VSV-G in post-ER compartments using electron microscopy, we employed two approaches as follows: semi-quantitative immunoperoxidase cytochemistry and quantitative immunoelectron microscopy.

BHK cells were transfected with either GFP-G^{ts}-DXE or GFP-G^{ts}-AXA at 39.5 °C and shifted to 32 °C for 120 min to reach a steady-state distribution in all cellular compartments. Subsequently, these cells were prepared for electron microscopy under identical conditions. By using immunoperoxidase

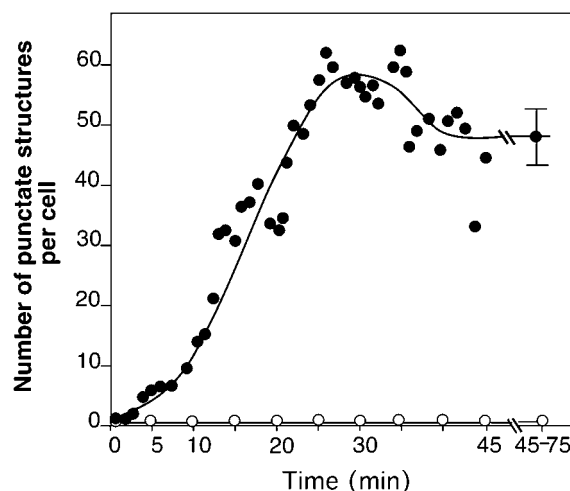


FIG. 5. Quantitation of appearance of VSV-G in punctate intermediates. The number of punctate intermediates containing GFP-G^{ts}-DXE (closed circles) or GFP-G^{ts}-AXA (open circles) with a greater than 2-fold increase in pixel intensity relative to the ER at 1-min intervals (closed circles) or 5-min intervals (open circles) is plotted. The 45–75-min time point is the averaged value of punctate intermediates observed in this time frame with the standard deviation of the mean indicated.

labeling with an antibody directed to the luminal domain of VSV-G, both GFP-G^{ts}-DXE and GFP-G^{ts}-AXA could be detected in a weak, diffuse distribution in the ER (Fig. 6, A–C, arrows). In cells transfected with GFP-G^{ts}-DXE, horseradish peroxidase (HRP) reaction products were heavily concentrated in Golgi compartments compared with the ER (Fig. 6A). In 25 transfected cells examined, 95% (96/101) of the Golgi stacks detected contained concentrated VSV-G throughout all cisternae. In contrast, cells transfected with the GFP-G^{ts}-AXA construct showed a uniformly weak deposition of HRP reaction product in the Golgi (Fig. 6, B and C). In 25 transfected cells containing VSV-G in the ER, 49% (48/98) of Golgi stacks contained minimally detectable levels of VSV-G in at least one of the Golgi compartments. Given the fact that the average expression level of GFP-G^{ts}-AXA is approximately 2-fold that of GFP-G^{ts}-DXE (Fig. 2A, inset in panel a), these results are completely consistent with the low levels of fluorescence in GFP-G^{ts}-AXA-expressing cells using light microscopy.

To quantitate the fold difference in concentration between GFP-G^{ts}-DXE and GFP-G^{ts}-AXA in the Golgi of transfected cells, we prepared cells as described above, and we determined the distribution of VSV-G using 6-nm gold particles in conjunction with cryoimmunoelectron microscopy and stereology (38). Typical images (Fig. 6D (GFP-G^{ts}-DXE) and E (GFP-G^{ts}-AXA)) revealed a striking difference in their relative concentrations. Whereas GFP-G^{ts}-DXE was present at an average concentration of 82 gold particles per μm^2 , GFP-G^{ts}-AXA was present at a concentration of 7.7 gold particles per μm^2 , corresponding to an ~10-fold difference. Given our previous results demonstrating that the level of concentration of VSV-G detected in Golgi compartments directly reflects the concentration of VSV-G in COPII vesicles exiting the ER (3, 24, 38), these data provide high resolution evidence for the importance of the DXE code in promoting concentration during ER export.

Export of GFP-G^{ts} from the ER Can Be Visualized in Real Time *In Vitro* Using Permeabilized Cells—In order to begin to gain biochemical insight into the concentration process, we developed a new approach to follow the real time movement of VSV-G into pre-Golgi intermediates *in vitro* using permeabilized cells. We have previously demonstrated the utility of permeabilized cells to follow morphologically the concentration

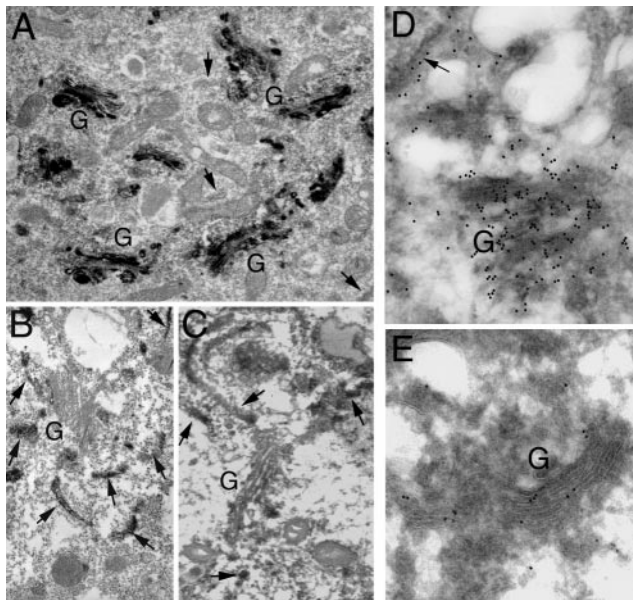


FIG. 6. Electron microscopy of steady-state concentration of GFP-G^{ts}-DXE and GFP-G^{ts}-AXA in the Golgi compartments. BHK cells were transfected with either GFP-G^{ts}-DXE (A and D) or GFP-G^{ts}-AXA (B, C, and E) at 39.5 °C. Following transfection, cells were shifted to 32 °C for 120 min to reach steady state. The distribution of VSV-G was visualized by immunoperoxidase staining as described under “Experimental Procedures” (A–C) or immunoelectron microscopy using 6-nm gold particles (D and E). D and E, visualization of the distribution of 6-nm gold particles has been enhanced by placement of a 12-nm dot over each gold particle. Arrows indicate the ER; G indicates Golgi complex.

of VSV-G into punctate structures that correspond to pre-Golgi intermediates observed *in vivo* (23, 24, 26, 38). By using this approach, we have shown that cargo selection involves the COPII budding machinery whose assembly is controlled by the activation of the Sar1 GTPase (3, 27, 38, 43).

To follow movement of VSV-G *in vitro*, normal rat kidney (NRK) cells expressing either GFP-G^{ts}-DXE or GFP-G^{ts}-AXA were incubated at 39.5 °C to retain VSV-G in the ER. Subsequently, the coverslip containing cells was transferred to ice, permeabilized, and incubated *in vitro* in the presence of cytosol and ATP. The movement of GFP-G^{ts} from the ER to post-ER compartments within the same cell was visualized using video microscopy following shift from 4 to 32 °C. Under these conditions, the transport of GFP-G^{ts}-DXE *in vitro* from the ER to pre-Golgi intermediates could be readily detected. At the first time point, corresponding to approximately 5 min after temperature shift (the time period required for acquisition of the first image), GFP-G^{ts}-DXE could be weakly detected in small fluorescence puncta indicative of initiation of ER export (Fig. 7A, arrowheads). By 20 min, numerous brightly fluorescent puncta were detected in GFP-G^{ts}-DXE-containing cells (Fig. 7A, arrowheads). In contrast, GFP-G^{ts}-AXA could not be detected in fluorescence puncta by the 60- (Fig. 7B) or 120-min time points (data not shown).

When quantitated (Fig. 7C), GFP-G^{ts}-DXE-containing puncta reach a maximum level of ~30–40 intermediates per cell by the 20-min time point. These results are consistent with the ~5-fold reduced kinetics of processing of GFP-G^{ts}-AXA to endo H-resistant forms *in vitro* compared with GFP-G^{ts}-DXE (data not shown). Therefore, cytosol and ATP-dependent export *in vitro* faithfully reconstitute the requirement for the DXE motif in concentration of VSV-G in pre-Golgi intermediates observed *in vivo*.

The Concentration Defect in GFP-G^{ts}-AXA Cannot Be Suppressed by the Addition of Activated Sar1-GTP—G^{ts}-AXA can

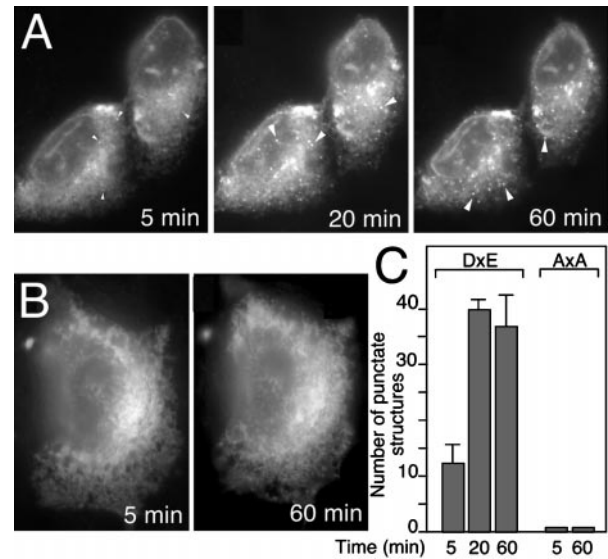


FIG. 7. Transport and concentration of GFP-G^{ts}-DXE in the pre-Golgi intermediates can be reconstituted *in vitro*. A, NRK cells expressing GFP-G^{ts}-DXE were permeabilized on ice and placed in ice-cold transport mixture. Transport was initiated by changing the temperature from 4 to 32 °C as described under “Experimental Procedures.” The first time point collected, reflecting technical limitations, corresponds to 5 min after temperature shift. Time-lapse images of VSV-G within a permeabilized cell were acquired for up to 120 min as described under “Experimental Procedures.” Transport in a typical cell (>50 cells examined) is shown. The arrowheads indicate pre-Golgi intermediates *in vitro*. NRK cells expressing GFP-G^{ts}-AXA were treated as in A. Transport in a typical cell (>50 cells examined) at the 5- and 60-min time points are shown. C, quantitation of the number of punctate intermediates containing GFP-G^{ts}-DXE or GFP-G^{ts}-AXA with a greater than 2-fold increase in pixel intensity relative to the ER at the indicated time points. The average value and standard deviation of the mean for 5 representative cells followed throughout an entire time course is shown.

be recruited to a pre-budding complex in the presence of the Sar1-GTP mutant at levels equivalent to G^{ts}-DXE yet fails to be concentrated before completion of COPII vesicle fission from the ER membrane. If the DXE-dependent concentration step is completed by the interaction between cargo and COPII components Sar1-GTP and Sec23/24, then the efficiency of recruitment of G^{ts}-AXA to pre-Golgi intermediates in permeabilized cells should be indistinguishable from G^{ts}-DXE when incubated in the presence of the Sar1-GTP mutant. Alternatively, if the concentration step utilizes additional factors recruited by the DXE signal, G^{ts}-AXA should not be concentrated in pre-Golgi intermediates as efficiently as G^{ts}-DXE. To address this issue, we incubated permeabilized cells with the Sar1-GTP mutant.

Incubation of permeabilized cells expressing GFP-G^{ts}-DXE in the presence of ATP, cytosol, and the Sar1-GTP mutant resulted in the appearance of concentrated VSV-G in numerous fluorescent puncta by 30 min of incubation (Fig. 8A, arrowheads). We have previously shown that these are composed of clusters of coated COPII vesicles due to the ability of the Sar1-GTP to prevent vesicle uncoating (3, 27, 38). In contrast, we were unable to detect GFP-G^{ts}-AXA in a concentrated form in pre-Golgi intermediates (Fig. 8A) at this early time point (30 min) when the AXA mutant can be fully recovered in pre-budding complexes containing the Sar1-GTP. This suggests that Sar1-GTP could not bypass inactivation of the DXE signal in the concentration step. However, at later time points (60 min) GFP-G^{ts}-AXA was detectable in punctate pre-Golgi intermediates (Fig. 8B, arrowheads). This lag is consistent with the 5–10-fold reduction in the kinetics of transport of G^{ts}-AXA from

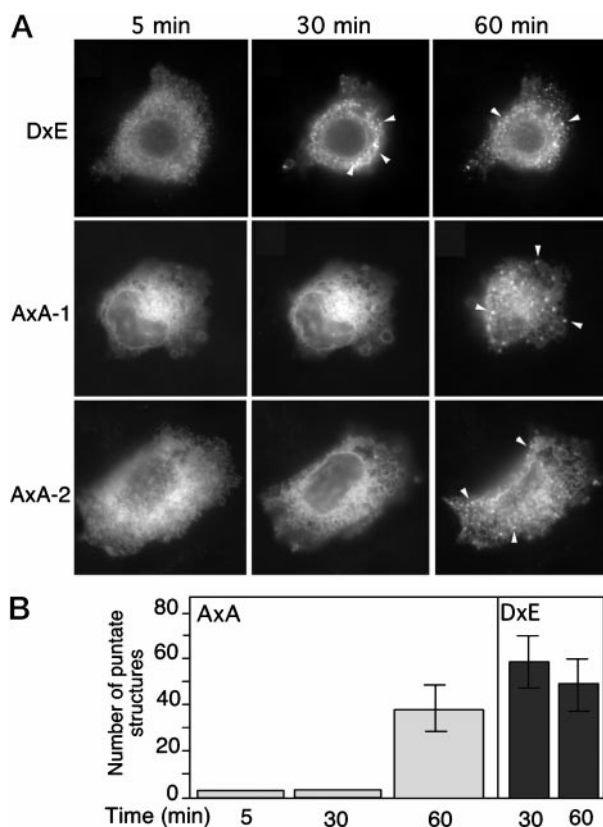


FIG. 8. The concentration defect in GFP-G^{ts}-AXA cannot be completely suppressed in the presence of the Sar1-GTP mutant *in vitro*. A, NRK cells expressing either GFP-G^{ts}-DxE (DxE) or GFP-G^{ts}-AXA (AXA-1 and AXA-2 (two representative cells shown)) were permeabilized on ice and placed in ice-cold transport mixture supplemented with 1 μ M activated Sar1-GTP (Sar1[H79G]). Transport was initiated by changing the temperature from 4 to 32 $^{\circ}$ C. Time-lapse images of VSV-G within a cell were acquired at 5 min and every 10 min thereafter for up to 120 min as described under "Experimental Procedures." Representative cells following at 5, 30, and 60 min of incubation are shown. The arrowheads indicate pre-Golgi vesicle clusters containing concentrated VSV-G. B, quantitation of the number of punctate intermediates containing GFP-G^{ts}-DxE or GFP-G^{ts}-AXA with a greater than 2-fold increase in pixel intensity relative to the ER at the indicated time points. The average value and standard deviation for 5 representative cells followed throughout an entire time course is shown.

the ER to Golgi *in vivo*. Thus, whereas activation of Sar1 to the GTP-bound form is necessary for cargo selection (3), it is not sufficient to rapidly concentrate VSV-G into COPII vesicles. This suggests that DxE signal plays an important role in recruiting an additional factor(s) that mediates cargo concentration for efficient ER export.

DISCUSSION

In the present study we have examined the biochemical role of the di-acidic code found in the cytoplasmic tail of VSV-G (14) in mediating the efficiency of export of cargo from the ER. We have now shown that the code is involved in a step involving concentration in COPII-coated vesicles. To demonstrate this point, we used combined biochemical and morphological approaches, in particular utilizing GFP-tagged VSV-G to visualize the ER export in real time. This approach allowed us to follow the fate of VSV-G in a single cell during trafficking from the ER to the cell surface *in vivo*. Moreover, we have now extended this technology to visualize the movement of GFP-G^{ts} *in vitro*. This facile approach gives us precise biochemical control over incubation conditions that are important to physiologically mobilize VSV-G from the ER (3, 27, 38). Our results provide new insight into the pathway directing export of cargo from the ER.

Role of DxE in Recovery of VSV-G in Pre-budding Complexes—We found that mutation of the DxE code to AXA does not affect the ability of VSV-G to be recovered in detergent-soluble pre-budding complexes formed *in vitro* in the presence of activated Sar1-GTP and purified Sec23/24 when the AXA mutant is largely present in the ER. This selection event is the first detectable step in the capture of VSV-G into COPII vesicles in mammalian cells (3) and for COPII vesicle assembly by endogenous recycling transport factors in yeast (44). Although we were at first surprised that the DxE code was not required for cargo selection by Sar1-GTP and Sec23/24, this result is entirely consistent with the fact that loss of the code affects the kinetics of transport but not the extent (14). We conclude that at least one principal activity that is responsible for the accelerated rate of VSV-G export from the ER is downstream from selection into pre-budding complexes. These results raise the possibility that the multiple signals may be required in VSV-G and other cargo for efficient export. Experiments are currently in progress to address this possibility.

DxE Is Involved in Concentration in COPII Vesicles—By using both indirect immunofluorescence and electron microscopy we have demonstrated an important role for the DxE motif in concentration of cargo in COPII vesicles. Evidence for this conclusion stems from the observation that the AXA mutant could not be detected in a concentrated form in pre-Golgi and Golgi compartments under a variety of incubation conditions designed to block and accumulate cargo in post-ER compartments at reduced temperature. Moreover, continuous monitoring of movement *in vivo* and *in vitro* failed to detect even a transient appearance of concentrated AXA mutant in the early secretory pathway over a time frame in which the AXA mutant is efficiently processed to endo H-resistant forms and delivered to the cell surface. Two independent approaches were used to characterize the concentration of VSV-G in post-Golgi compartments using electron microscopy. Given the fact that the concentration of VSV-G in Golgi compartments is a measure of concentration during ER export (3, 24, 38), the reduced level of HRP reaction product or gold particles in Golgi compartments expressing the AXA mutant when compared with wild-type demonstrates a marked deficiency in concentration during COPII vesicle budding. It is apparent that inactivation of the code (mutation of DxE to AXA) uncouples VSV-G from the concentration machinery *in vivo*.

Requirement for Sar1-GTP in Cargo Concentration—Because we could not detect a difference in the recovery of wild-type VSV-G or the AXA mutant in pre-budding complexes formed in the presence of Sar1-GTP, we examined whether Sar1-GTP could bypass the concentration defect following inactivation of the code. We found that this was not the case. Incubation in the presence of Sar1-GTP did not result in normal concentration of the AXA mutant. At early time points (30 min), when wild-type VSV-G could be readily detected in a concentrated form in pre-Golgi intermediates in the presence of Sar1-GTP, the AXA mutant could not be detected. This result is consistent with the reduced kinetics of export of the AXA mutant (14). Because recruitment to pre-budding complexes by Sar1-GTP appears unaffected in the AXA mutant under the current experimental conditions, it is apparent that concentration is a distinct step in the export pathway. These results emphasize that the DxE code is essential for rapid concentration even in the presence of the activated Sar1-GTP mutant.

In contrast to early time points, we found that at later time points (60 min), the AXA mutant could start to be detected in a concentrated form in pre-Golgi intermediates in the presence of Sar1-GTP. This result contrasts to normal incubation conditions (in the presence of wild-type Sar1) where the AXA mutant

could not be detected in pre-Golgi intermediates or Golgi compartments even after 120 min of incubation. Suppression of the AXA mutant phenotype at later time points is not due to a general loss of fidelity in cargo selection, as we have previously documented that Sar1-GTP has no effect on the ability of resident ER proteins to be efficiently excluded from COPII vesicles formed *in vitro* (3, 27). One possibility to explain concentration at late time points is that incubation with Sar1-GTP favors stable recruitment of COPII components to ER membranes (1, 3, 45). This increase in the steady-state level of the COPII components on the ER surface could result in efficient "capture" of lower affinity AXA mutant without additional DXE signal-dependent factors. An alternative, but very speculative possibility, is that the DXE code normally facilitates coat assembly by stabilizing Sar1 in the GTP-bound form upon assembly of a "recruitment" complex, thereby facilitating efficient packing of cargo by COPII complexes.

The ability of excess Sar1-GTP to alter the efficiency of recruitment of wild-type and mutant biosynthetic cargo is consistent with recent observations from biochemical analysis of yeast COPII components in vesicle budding. First, COPII vesicle budding from artificial liposomes requires ~5-fold higher concentration of activated Sar1 than that required to generate vesicles using microsomes (45). This suggests that the liposomes form a low affinity template for COPII coat assembly. *In vivo*, biosynthetic and/or recycling cargo would be expected to initiate these events (3, 32, 44). Second, the incorporation of biosynthetic cargo and recycling cargo into COPII vesicles is differentially affected by the amount of Sar1 (46). Thus, exported proteins require different levels of COPII components for efficient export, suggesting recruitment is affected by the relative affinity of the protein for the COPII machinery.

Sequential Steps Direct Pre-budding Complex Formation and Concentration—We have shown that recruitment of VSV-G to COPII vesicles involves selection into pre-budding complexes containing Sar1-GTP and Sec23/24 (3) that is DXE-independent (this study). This is followed by a DXE-dependent concentration step, suggesting that mutation of the DXE signal can uncouple selection from concentration. We propose that DXE may serve as a high affinity recruitment motif for a novel "linker" component(s), possibly SNARE proteins that have recently been shown to bind to Sar1 *in vitro* (44), or it may enhance recruitment of membrane-associated components such as Sec16 that interact with Sec23/24 and whose role in COPII vesicle assembly remain to be defined (47–49). Alternatively, it may recruit presently unknown factors that stabilize the formation of pre-budding complexes or mediate stable coat assembly from pre-budding complexes. Our combined results suggest for the first time that export from the ER may involve at least a two-step mechanism. In this model, cargo present in pre-budding complexes (Fig. 9, *step 1*) undergoes a distinct concentration event for efficient recruitment to COPII vesicles (Fig. 9, *step 2*).

The two-step model is supported by three lines of evidence. First, the inactivation of the DXE can distinguish pre-budding complex formation from concentration processes. Second, these two steps have different sensitivities for the activated Sar1-GTP mutant. Whereas G^{ts} -AXA can be recovered in pre-budding complexes containing the Sar1-GTP mutant as efficiently as G^{ts} -DXE, the inefficient kinetics of concentration in pre-Golgi intermediates observed in the G^{ts} -AXA mutant cannot be restored to normal efficiency by incubation in the presence of the Sar1-GTP. This argues that following an initial interaction between VSV-G and a subset of COPII components, further step(s) are required to promote a concentration event that requires DXE-dependent factors. Third, when G^{ts} -DXE con-

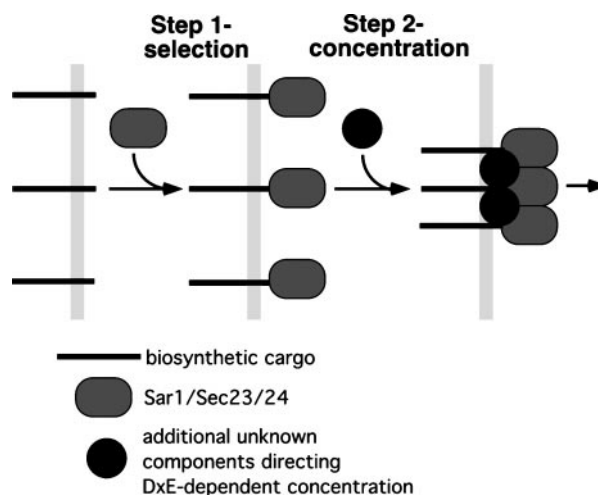


FIG. 9. Model for the mechanism of DXE function in export from the ER. In a two-step mechanism of cargo export from the ER, an initial event directing assembly of partial (pre-budding) coat complexes is augmented by a separate DXE-dependent second step that directs concentration of cargo through the activity of additional factors.

taining microsomes are retained at the restrictive temperature (where G^{ts} is unfolded and remains in a diffuse ER reticular distribution), G^{ts} -DXE can be efficiently recovered in pre-budding complexes (32). This provides an independent line of evidence that cargo selection can be uncoupled from concentration. Furthermore, a number of endogenous accessory factors, some of which recycle between the ER and Golgi, are now recognized to be essential for the export of specific biosynthetic cargo proteins, for example NinaA, receptor-associated protein, Shr3, and p53/58 that are required for ER export of rhodopsin, low density lipoprotein receptor-related proteins, general amino acid permease-1, and procathepsin C, respectively (18, 22, 50, 51). Although their mechanism of action is currently unknown, it is possible that these factors regulate either selection (*step 1*), concentration (*step 2*), or novel, unidentified steps prior to COPII vesicle formation.

Export from the ER requires discrimination between immature and mature cargo by the COPII machinery. The use of a multi-step pathway allows for branch points in which dysfunctional cargo can be targeted for degradation. Moreover, it provides additional flexibility of the rate in which different forms of cargo are exported from the ER, perhaps independent of their folding pathways. Such a multi-step pathway may be applicable to clathrin-mediated endocytosis of cell-surface receptors. For example, stimulation of the β_2 -adrenogenic receptor triggers recruitment of β -arrestin from cytosol and regulates the concentration of receptor in clathrin-coated vesicles (52). We have recently demonstrated that cargo selection by Sar1-GTP and Sec23/24 is an early event, as even the misfolded form of G^{ts} can be recovered in pre-budding complexes at the restrictive temperature (32). These results demonstrate that cargo can modulate general COPII vesicle formation from the ER through competition for general transport factors that may participate in later steps of COPII vesicle assembly (32). Studies currently in progress directed at identifying the component(s) that mediate DXE-dependent cargo concentration in the ER should provide important insight into such mechanisms.

Acknowledgment—We thank K. Mostov for generous support of adenovirus vector construction.

REFERENCES

1. Aridor, M., and Balch, W. E. (1996) *Trends Cell Biol.* **6**, 315–320
2. Schekman, R., and Orci, L. (1996) *Science* **271**, 1526–1533

3. Aridor, M., Weissman, J., Bannykh, S., Nouffer, C., and Balch, W. E. (1998) *J. Cell Biol.* **141**, 61–70
4. Kuehn, M. J., Herrmann, M., and Schekman, R. (1998) *Nature* **391**, 187–190
5. Schmid, S. L. (1997) *Annu. Rev. Biochem.* **66**, 511–548
6. Bonifacino, J. S., Marks, M. S., Ohno, H., and Kirchhausen, T. (1996) *Proc. Assoc. Am. Physicians* **4**, 285–295
7. Jackson, M. R., Nilsson, T., and Peterson, P. A. (1990) *EMBO J.* **9**, 3153–3161
8. Cosson, P., and Letourneur, F. (1997) *Curr. Opin. Cell Biol.* **9**, 484–487
9. Harter, C., and Wieland, F. T. (1998) *Proc. Natl. Acad. Sci. U. S. A.* **95**, 11649–11654
10. Kappeler, F., Klopfenstein, D. R. Ch., Foguet, M., Paccaud, J. P., and Hauri, H. P. (1997) *J. Biol. Chem.* **272**, 31801–31808
11. Dominguez, M., Dejgaard, K., Fullekrug, J., Dahan, S., Fazel, A., Paccaud, J.-P., Thomas, D. Y., Bergeron, J. J. M., and Nilsson, T. (1998) *J. Cell Biol.* **140**, 751–765
12. Fiedler, K., Veit, M., Stamnes, M. A., and Rothman, J. E. (1996) *Science* **273**, 1396–1399
13. Nakamura, N., Yamazaki, S., Sato, K., Nakano, A., Sakaguchi, M., and Mihara, K. (1999) *Mol. Biol. Cell* **9**, 3493–3503
14. Nishimura, N., and Balch, W. E. (1997) *Science* **277**, 556–558
15. Bannykh, S., Nishimura, N., and Balch, W. E. (1998) *Trends Cell Biol.* **8**, 21–25
16. Hurtley, S. M., and Helenius, A. (1989) *Annu. Rev. Cell Biol.* **5**, 277–307
17. Kopito, R. R. (1997) *Cell* **88**, 427–430
18. Kuehn, M. J., Schekman, R., and Ljungdahl, P. O. (1996) *J. Cell Biol.* **135**, 585–595
19. Colley, N. J., Cassill, J. A., Baker, E. K., and Zuker, C. S. (1995) *Proc. Natl. Acad. Sci. U. S. A., U. S. A.* **92**, 3070–3074
20. Nichols, W. C., Seligsohn, U., Zivelin, A., Terry, V. H., Hertel, C. E., Wheatley, M. A., Moussalli, M. J., Hauri, H. P., Ciavarella, N., Kaufman, R. J., and Ginsburg, D. (1998) *Cell* **93**, 61–70
21. Schimmoller, F., Singer-Kruger, B., Schroder, S., Kruger, U., Barlowe, C., and Riezman, H. (1995) *EMBO J.* **14**, 1329–1339
22. Vollenweider, F., Kappeler, F., Itin, C., and Hauri, H.-P. (1998) *J. Cell Biol.* **142**, 377–389
23. Aridor, M., Bannykh, S. I., Rowe, T., and Balch, W. E. (1995) *J. Cell Biol.* **131**, 875–893
24. Balch, W. E., McCaffery, J. M., Plutner, H., and Farquhar, M. G. (1994) *Cell* **76**, 841–852
25. Beckers, C. J. M., Keller, D. S., and Balch, W. E. (1987) *Cell* **50**, 523–534
26. Plutner, H., Davidson, H. W., Saraste, J., and Balch, W. E. (1992) *J. Cell Biol.* **119**, 1097–1116
27. Rowe, T., Aridor, M., McCaffery, J. M., Plutner, H., and Balch, W. E. (1996) *J. Cell Biol.* **135**, 895–911
28. Dascher, C., and Balch, W. E. (1996) *J. Biol. Chem.* **271**, 15866–15869
29. Altschuler, Y., Barbas, S. M., Terlecky, L. J., Tang, K., Hardy, S., Mostov, K. E., and Schmid, S. L. (1998) *J. Cell Biol.* **143**, 1871–1881
30. Heim, R., Cubitt, A. B., and Tsien, R. Y. (1995) *Nature* **373**, 663–664
31. Higuchi, R., Krummel, B., and Saiki, R. K. (1988) *Nucleic Acids Res.* **16**, 7351–7367
32. Aridor, M., Bannykh, S. I., Rowe, T., and Balch, W. E. (1999) *J. Biol. Chem.* **274**, 4389–4399
33. Lafay, F. (1974) *J. Virol.* **14**, 1220–1228
34. Rowe, T., Dascher, C., Bannykh, S., Plutner, H., and Balch, W. E. (1998) *Science* **279**, 696–700
35. Presley, J. F., Cole, N. B., Schroer, T. A., Hirschberg, K., Zaal, K. J. M., and Lippincott-Schwartz, J. (1997) *Nature* **389**, 81–84
36. Velasco, A., Henricks, L., Moreman, K. W., Tulsiani, D. R. P., Touster, O., and Gist Farquhar, M. (1993) *J. Cell Biol.* **122**, 39–51
37. Schwaninger, R., Beckers, C. J. M., and Balch, W. E. (1991) *J. Biol. Chem.* **266**, 13055–13063
38. Bannykh, S. I., Rowe, T., and Balch, W. E. (1996) *J. Cell Biol.* **135**, 19–35
39. Griffiths, G., Fuller, S. D., Back, M., Hollinshead, M., Pfeiffer, S., and Simons, K. (1989) *J. Cell Biol.* **108**, 277–297
40. Saraste, J., and Svensson, K. (1991) *J. Cell Sci.* **100**, 415–430
41. Saraste, J., and Kuismanen, E. (1984) *Cell* **38**, 535–549
42. Schweizer, A., Fransen, J. A. M., Bachi, T., Ginsel, L., and Hauri, H.-P. (1988) *J. Cell Biol.* **107**, 1643–1653
43. Kuge, O., Dascher, C., Orci, L., Rowe, T., Amherdt, M., Plutner, H., Ravazzola, M., Tanigawa, G., Rothman, J. E., and Balch, W. E. (1994) *J. Cell Biol.* **125**, 51–65
44. Springer, S., and Schekman, R. (1998) *Science* **281**, 698–700
45. Matsuoka, K., Orci, L., Amherdt, M., Bednarek, S. Y., Hamamoto, S., Schekman, R., and Yeung, T. (1998) *Cell* **93**, 263–275
46. Campbell, J. L., and Schekman, R. (1997) *Proc. Natl. Acad. Sci. U. S. A.* **94**, 837–842
47. Gimeno, R. E., Espenshade, P., and Kaiser, C. A. (1996) *Mol. Biol. Cell* **7**, 1815–1823
48. Shaywitz, D. A., Espenshade, P. J., Gimeno, R. E., and Kaiser, C. A. (1997) *J. Biol. Chem.* **272**, 25413–25416
49. Espenshade, P., Gimeno, R. E., Holzmacher, E., Teung, P., and Kaiser, C. A. (1995) *J. Cell Biol.* **131**, 311–324
50. Colley, N. J., Baker, E. K., Stamnes, M. A., and Zuker, C. S. (1991) *Cell* **67**, 255–263
51. Bu, G., and Schwartz, A. L. (1998) *Trends Cell Biol.* **8**, 272–276
52. Luttrell, L. M., Ferguson, S. S. G., Daaka, Y., Miller, W. E., Maudsley, S., Della Rocca, G. J., Lin, F., Kawakatsu, H., Owada, K., Luttrell, D. K., Caron, M. G., and Lefkowitz, R. J. (1999) *Science* **283**, 655–661